Numerical Analysis of Cellular Detonation Frontal Structure in Liquid *n*-Dodecane Sprays

Qingyang Meng[1,2], Liangqi Zhang[2], Huangwei Zhang[3]
[1] National University of Singapore (Chongqing) Research Institute
Chongqing, Chongqing, People's Republic of China
[2] College of Aerospace Engineering, Chongqing University
Chongqing, Chongqing, People's Republic of China
[3] Department of Mechanical Engineering, National University of Singapore
Republic of Singapore

1 Introduction

Liquid-fueled detonation has attracted great interests for aerospace propulsion in recent years since the high energy density of liquid fuel meets the weight/volume-limited requirement for aircraft. In comparison with gaseous detonation, spray detonation is still not fully developed because of the comparatively complicated detonation process [1], for instance, atomization, droplet breakup, vaporization, and shock-droplet interaction. In particular, the breakup and vaporization significantly lengthen the reaction zone length, and the heat absorption from the vaporization deteriorates the coupling between the leading shock front and the reaction zone, which makes the spray detonation presents a relatively low detonability compared with gaseous detonation, especially for complicated hydrocarbon fuels [2]. In this regard, different approaches for detonability enhancement are used in the spray detonation, such as pre-vaporization [2, 3], oxidant pre-heating [4], atomization optimization [5], which would result in different detonation cellular structures related to complicated physical or chemical mechanisms. Clarifying the feature of the detonation cellular structure is helpful to develop the fundamental theory of spray detonation, and facilitate the optimization of the operation and performance for the practical application. In this work, we investigate the spray detonation characteristics in the *n*-dodecane/oxygen/nitrogen mixture under different initial temperatures and some preliminary results will be presented.

2 Methodology

The equations of mass, momentum, energy and species mass fraction are solved by a well-validated OpenFOAM solver *RYrhoCentralFoam* [2, 6, 7]. The second-order backward scheme is employed for temporal discretization and the time step is about 5×10^{-10} s. A MUSCL-type upwind-central scheme [8] with van Leer limiter is used for calculating the convective fluxes in the momentum equation. The second-order central differencing scheme is applied for the diffusion terms in all equations. A skeletal *n*-dodecane mechanism with 54 species and 269 reactions [9] is used. The chemistry is integrated with

Correspondence to: huangwei.zhang@nus.edu.sg

the implicit Euler method. Mono-dispersed droplets are considered, and the droplet breakup process is modelled following Pilch and Erdman [10].

3 Physical problem

A two-dimensional configuration is used in this study, as shown in Fig. 1. The streamwise (*x*-direction) and spanwise (*y*-direction) length of the domain are 1.0 m and 0.05 m, respectively. The left and right boundaries are non-reflective, and the upper and lower ones are periodic. The initial pressure (p_0) is 1.0 atm in the two-phase section, and the oxidant is oxygen/nitrogen mixture with 1:1 by mass. Different initial temperatures (T_0), i.e., 300 K and 600 K, are studied in the two-phase section. Pure *n*-dodecane sprays with the initial droplet diameter (d_0) of 5 μm and temperature (T_d) of 300 K are considered, and the liquid equivalence ratio (ϕ_l) is unity in the two-phase section, which is defined as the mass ratio of liquid fuel to oxidant normalized by it on stoichiometric condition. A freely propagating detonation wave is established from the stoichiometric gaseous *n*-dodecane mixture in the detonation development section (see Fig. 1). Three hot spots are imposed along the spanwise direction in the leftmost end with temperature of 2,000 K and pressure of 50 atm for initializing the detonation. A freely propagating DW can be achieved when *x* is greater than about 0.5 m. Our analysis in this paper is based on the two-phase section of 0.8−1.0 m, which are discretized with 4,000,000 uniform Cartesian cells (mesh size of $\Delta x = \Delta y = 50$ μm).

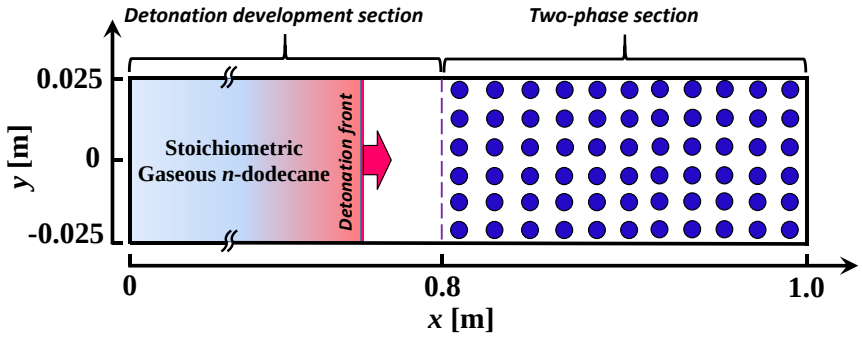

Figure 1: Schematic of computational domain.

4 Results and discussion

4.1 Cellular structure feature

The cellular feature of spray detonation with initial temperature of 600 K is presented in Fig. 2 by displaying the contours of key gas and liquid droplet quantities. A stable detonation wave (DW) is found, featured by the numerous triple points (TP) along the leading shock front (SF). The strong DW leads to a significantly short dispersion distance behind the SF as seen in Fig. 2(a), which also results from the droplet breakup induced by the shock, and hence the droplet diameter quickly reduces to about 0.08 μm from 5 μm. Besides, early vaporization of the droplet caused by the relatively high temperature is responsible for the short dispersion distance, and it can be found in Fig. 2(b) that the mass ratio of gaseous *n*-dodecane to oxidant (F/O) is about 0.2 ahead of the SF due to the early vaporization. In addition, the non-uniform temperature distribution originates from the different reaction progresses caused by the different shock strengths from Mach stem (MS) and incident wave (IW), supported by the corresponding distributed heat release rate (HRR) in Fig. 2(c). Due to the small initial diameter (i.e., 5 μm), the droplets can be quickly heated up to about 658 K, as shown in Fig. 2(d). In addition, one can find that the droplet evaporation rate ($\dot{m}_d$) presents a spotty distribution along the SF. The high evaporation rate is found behind the MS, whereas the low one behind the IW in Fig. 2(e).

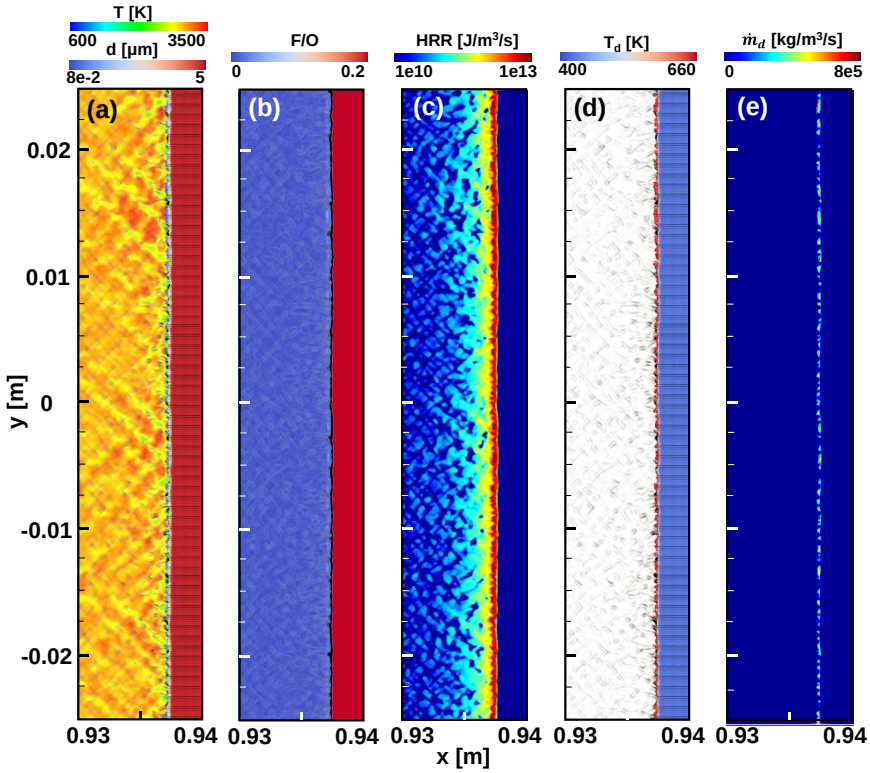

Figure 2: Contours of (a) gas temperature overlaid by the droplets colored by diameter, (b) mass ratio of gaseous *n*-dodecane to oxidant, (c) heat release rate, (d) droplets colored by temperature (T_d), and (e) evaporation rate $\dot{m}_d$. Logarithmic scale legend is used in HRR contours. Contours of pressure gradient magnitude are visualized in Figs. (a)−(d). T_0 = 600 K.

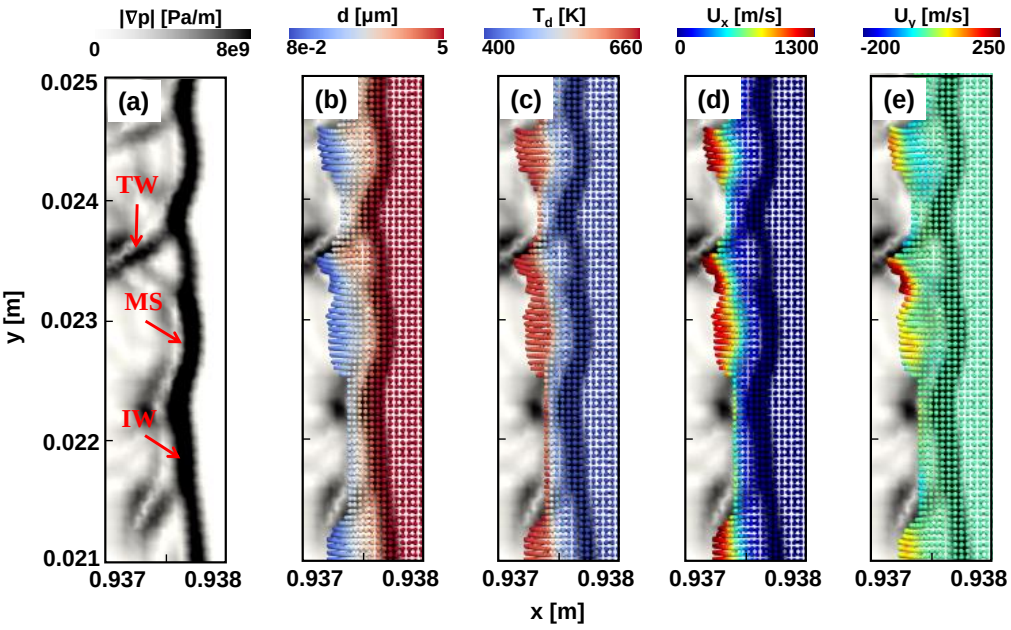

Figure 3: Contours of (a) pressure gradient magnitude, local droplet distribution colored by (b) diameter, (c) temperature, (d) droplet velocity in *x*-component direction, and (e) droplet velocity in *y*-component direction. Contours of pressure gradient magnitude are visualized in Figs. (b)−(e). T_0 = 600 K.

Local detonation frontal structure and the corresponding droplet distribution with different parameters are shown in Fig. 3. The typical detonation structure, such as MS, IW and transverse wave (TW), can be found. Moreover, different dispersion distances behind the MS and IW are noticed because of the different shock impacts on the breakup event. Specifically, before the moment in Fig. 3, droplets penetrate through the IW with relatively low evaporation rate and long breakup time, when this IW transforms into the MS in a very short time due to the frequent TP collision, a long dispersion distance has formed. In contrast, evidently short dispersion distance is seen behind the IW because the small child droplets have been quickly heated up to about 658 K due to their smallness as seen in Fig. 3(c), and these small droplets also exhibit high *x*-component velocity in Fig. 3(d) because of their shorter momentum response time. The transverse movement of the child droplets evidenced by the positive and negative *y*-component velocities demonstrates the effects of TW on them as seen in Fig. 3(e).

The results with T_0 decreased to 300 K are presented in a similar configuration to that in the case of T_0 = 600 K as seen in Fig. 4 and Fig. 5. The extinction is observed, confirmed by the noticeable decoupled RF and SF in Figs. 4(a) and 4(c). The MS or IW is difficult to be identified in Fig. 5(a) due to the weak SF, and the dispersion distance difference is insignificant along the SF as seen in Figs. 5(d)−(e), where the droplet velocity difference is lower than that in Figs. 3(d)−(e). Besides, in the lengthened induction zone, considerable unburned *n*-$C_{12}H_{26}$ vapor can be found according to the high F/O in Fig. 4(b), which stems from the droplet vaporization in the vicinity of the SF. Moreover, the absence of *n*-dodecane vapor ahead of DW results from the same initial temperature between the droplet and gas. The evaporation rate when T_0 = 300 K is evidently lower than that when T_0 = 600 K, and the dispersion distance is relatively longer, which can be clearly noticed in Figs. 5(b)−(e).

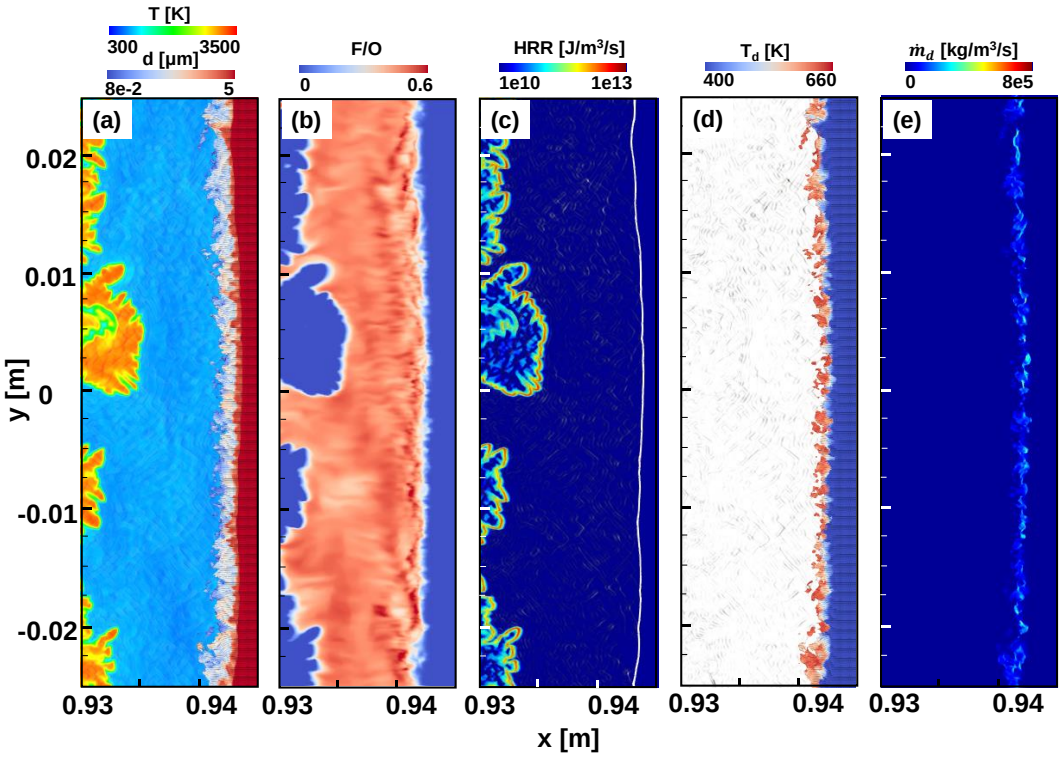

Figure 4: Contours of (a) gas temperature overlaid by the droplet colored by diameter, (b) mass ratio of gaseous *n*-dodecane to oxidant, (c) heat release rate, (d) droplet colored by temperature (T_d), and (e) evaporation rate $\dot{m}_d$. Logarithmic scale legend is used in HRR contours. Contours of pressure gradient magnitude are visualized in Figs. (a)−(d). T_0 = 300 K.

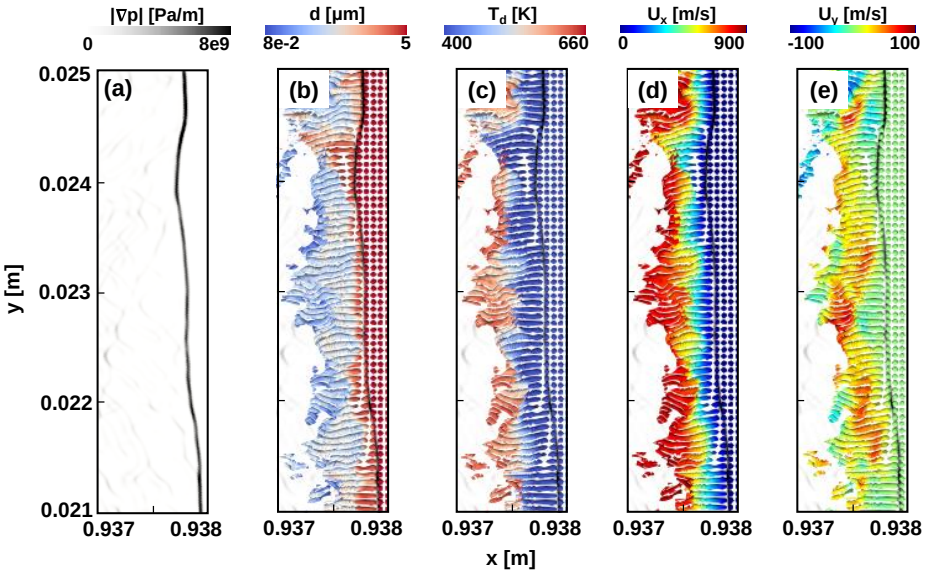

Figure 5: Contours of (a) pressure gradient magnitude, local droplet distribution colored by (b) diameter, (c) temperature, (d) droplet velocity in *x*-component direction, (e) droplet velocity in *y*-component direction. Contours of pressure gradient magnitude is visualized in Figs. (b)−(e). T_0 = 300 K.

4.2 Detonation speed

Figure 6 plots the detonation propagation speed in the two-phase section. When the initial gas temperature is T_0 = 600 K, a slight speed decrease is found because of the energy absorption from vaporization and droplet breakup. After about x = 0.85 m, the detonation speed slowly increases with distance since the high initial gas temperature leads to the early vaporization before DW arrival, which creates a pre-vaporization background gas, and hence the speed is very close to the corresponding Chapman−Jouguet (CJ) speed when the DW approaches x = 1.0 m. For case of T_0 = 300 K, a substantial speed decrease is found when DW enters the two-phase section since the extinction takes place, and a significant speed deviation from the CJ value is seen as DW approaches x = 1.0 m.

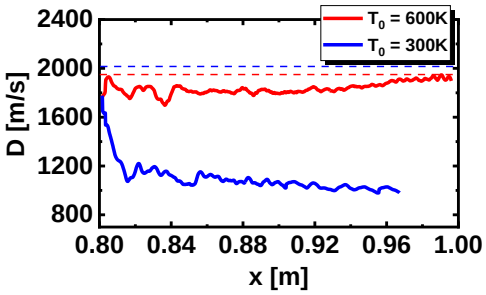

Figure 6: Time history of detonation speed under different initial temperatures. Dashed lines indicate the corresponding theoretical CJ values.

5 Conclusion

In this paper, the effects of gas initial temperature on the *n*-dodecane detonation cellular structure are investigated, and the results show that the initial temperature has a significant impact on detonation. Detonation wave stably propagates in the two-phase section when T_0 is 600 K since the relatively high initial temperature increases the evaporation rate, and facilitates the early vaporization before DW arrival. In addition, more child droplets exist behind the Mach stem than those behind the incident wave

because the breakup of penetrated droplet proceeds until the incident wave transforms into the Mach stem, resulting in different dispersion distances behind the shock front. In comparison with case of T_0 = 600 K, the extinction is observed when T_0 decreases to 300 K. More droplets are found behind the leading shock front with similar dispersion distance because of the weak shock front. Moreover, the lengthened induction zone for case of T_0 = 300 K is filled with considerable unburned *n*-dodecane vapor generated by the vaporized droplet in the vicinity of the shock front.

Higher initial gas temperature facilitates the increase of detonation speed as the detonation wave propagates in a two-phase atmosphere where the gas temperature is higher than that of droplet, and the two-phase detonation features gradually become similar to the gaseous detonation because more droplets gasify as their resident time increases in the high temperature medium.

Acknowledgement

The work used the computational resources from the supercomputer Fugaku in High-Performance Computing Infrastructure in Japan (hp210325). This work is supported by Chongqing Postdoctoral Science Foundation (No. CSTB2022NSCQ-BHX0023). QM is supported by College of Aerospace Engineering of Chongqing University and National University of Singapore (Chongqing) Research Institute.

References

[1] Kailasanath K. (2006). Liquid-fueled detonations in tubes. J. Propul. Power. 22: 1261.

[2] Meng Q, Zhao M, Xu Y, Zhang L, Zhang H. (2023). Structure and dynamics of spray detonation in *n*-heptane droplet/vapor/air mixtures. Combust. Flame. 249: 112603.

[3] Zhao M, Zhang H. (2021). Rotating detonative combustion in partially pre-vaporized dilute *n*-heptane sprays: Droplet size and equivalence ratio effects. Fuel. 304: 121481.

[4] Jin S, Xu C, Zheng H, Zhang H. (2022). Detailed chemistry modeling of rotating detonations with dilute *n*-heptane sprays and preheated air. Proc. Combust. Inst.

[5] Nair AP, Keller AR, Morrow DS, Lima AB, Mitchell Spearrin R, Pineda DI. (2022). Hypergolic Continuous Detonation with Space-Storable Propellants and Additively Manufactured Injector Design. J. Spacecraft Rockets. 59: 1332.

[6] Huang Z, Zhao M, Xu Y, Li G, Zhang H. (2021). Eulerian-Lagrangian modelling of detonative combustion in two-phase gas-droplet mixtures with OpenFOAM: Validations and verifications. Fuel. 286: 119402.

[7] Y. Xu, Zhao M, Zhang H. (2021). Extinction of incident hydrogen/air detonation in fine water sprays. Phys. Fluids. 33: 116109.

[8] Kurganov A, Noelle S, Petrova G. (2001). Semidiscrete central-upwind schemes for hyperbolic conservation laws and hamilton-jacobi equations. Siam J. Sci. Comput. 23: 707.

[9] Yao T, Pei Y, Zhong B-J, Som S, Lu T, Luo KH. (2017). A compact skeletal mechanism for n-dodecane with optimized semi-global low-temperature chemistry for diesel engine simulations. Fuel. 191: 339.

[10] Pilch M, Erdman CA. (1987). Use of Breakup Time Data and Velocity History Data to Predict the Maximum Size of Stable Fragments for Acceleration-Induced Breakup of a Liquid Drop. Int. J. Multiphas. Flow. 13: 741.